

## Synthesis, characterization, OFET and electrochemical properties of novel dimeric metallophthalocyanines

Cite this: *Dalton Trans.*, 2013, **42**, 6633Lale Meyancı Özer,<sup>a</sup> Metin Özer,<sup>a</sup> Ahmet Altındal,<sup>\*b</sup> Ali Rıza Özkaya,<sup>a</sup> Bekir Salih<sup>c</sup> and Özer Bekaroğlu<sup>\*d</sup>

The synthesis of 4,4'-[6,6'-methylenebis(2-(2-(3,4-dicyanophenoxy)-5-methylbenzyl)-4-methyl-6,1-phenylene)] bis(oxy) diphthalonitrile **1** was achieved starting from 4-nitrophthalonitrile and 6,6'-methylenebis(2-(2-hydroxy-5-methylbenzyl)-4-methylphenol) in DMF at 50 °C by the catalysis of K<sub>2</sub>CO<sub>3</sub> under argon. The corresponding dimeric metallophthalocyanines (Zn<sub>2</sub>Pc<sub>2</sub> **2** and Co<sub>2</sub>Pc<sub>2</sub> **3**) were tetramerized in dimethylaminoethanol with the appropriate metal salt. Newly synthesized compounds were characterized by elemental analysis, UV-vis, FT-IR (ATR), MALDI-TOF mass and <sup>1</sup>H-NMR spectroscopy techniques. The electrochemical properties of the complexes were examined by cyclic voltammetry, differential pulse voltammetry, controlled potential coulometry and *in situ* spectroelectrochemistry in nonaqueous media. The results showed that while there is considerable weak interactions between the two metal phthalocyanine units in dimeric zinc phthalocyanine, these interactions in dimeric cobalt phthalocyanine is remarkable. The catalytic performances of dimeric cobalt phthalocyanine in the reduction of oxygen in a medium similar to the working conditions of the polymer electrolyte membrane fuel-cells were found to be much higher than that of dinuclear zinc phthalocyanine. Solution-processed films of the complexes were utilized as an active semiconducting layer in the fabrication of organic field-effect transistors (OFETs) in the bottom-gate configurations. The output characteristics of the resulting p-type OFET devices were investigated to evaluate the performances such as the field effect mobility ( $\mu_F$ ). A relatively high field effect mobility of  $7.3 \times 10^{-3} \text{ cm}^2 \text{ V}^{-1} \text{ s}^{-1}$  was observed for dimeric cobalt phthalocyanine.

Received 21st January 2013,  
Accepted 18th February 2013

DOI: 10.1039/c3dt50212k

[www.rsc.org/dalton](http://www.rsc.org/dalton)

### 1. Introduction

For a couple of decades, mononuclear phthalocyanines (Pcs) have been the issue of an intensive study in multidisciplinary fields.<sup>1</sup> Cofacial sandwich type Pc dimers have been known since the first quarter of twentieth century, though the first planar dimer was reported at the end of the aforementioned century.<sup>2</sup> Since then, many papers have been published on both cofacial Pc dimers<sup>3</sup> and planar homodimers of Pc and Pc derivatives.<sup>4</sup> Furthermore, a large number of a new class of dimeric complexes, ball type Pcs which are covalently bonded with each other were reported. Owing to different bridges such as *tert*-butylcalix[4]arene,<sup>5</sup> 1,1'-methylene-dinaphthalen-2-ol,<sup>6</sup> pentaerythritol<sup>7</sup> and

its different derivatives,<sup>8</sup> 1a,8b-dihydronaphtho[*b*]naphthofuro[3,2-*d*]furan-7,10-diol,<sup>9</sup> phenolphthalein,<sup>10</sup> 9,9'-bis(4-hydroxyphenyl)fluorine,<sup>11</sup> 4,4'-(octahydro-4,7-methano-5*H*-inden-5-ylidene)-bisphenol,<sup>12</sup> and dicumarol,<sup>13</sup> syntheses of various ball-type metallophthalocyanines (MPcs) were achieved.

Dinuclear Pcs show a wide range of interactions between the Pc rings, mainly depending on the metal center, bridging links and the presence or absence of axial ligands. The dimers having flexible bridging units usually do not exhibit any measurable interaction, while rigid systems such as the anthracene and naphthalene bridged species do, however, exhibit strong interactions.<sup>14</sup> We also detected a strong interaction between the face-to-face Pc rings or two metal centers in ball-type complexes with spectroscopic and electrochemical evidence.<sup>15</sup> These novel compounds showed interesting mixed-valence behaviour, electrical and optical properties due to these interactions. The fact that even small modifications may lead to important changes in Pc characteristics and our continuing efforts in the design of novel macrocycles with potential applicability in various technological areas prompted us to synthesize new examples of dinuclear MPcs.

Organic field effect transistors (OFETs) act as key components for the next generation of cheap and flexible organic

<sup>a</sup>Department of Chemistry, Marmara University, 34722 Göztepe-Istanbul, Turkey. E-mail: [lmeyanci@marmara.edu.tr](mailto:lmeyanci@marmara.edu.tr), [metinozer@marmara.edu.tr](mailto:metinozer@marmara.edu.tr), [aliozkaya@marmara.edu.tr](mailto:aliozkaya@marmara.edu.tr); Fax: +90 216 3478783; Tel: +90 216 3479641

<sup>b</sup>Department of Physics, Davutpaşa Caddesi, 34220, Esenler, Istanbul, Turkey. E-mail: [altindal@yildiz.edu.tr](mailto:altindal@yildiz.edu.tr); Fax: +90 212 383 42 34; Tel: +90 212 383 42 31

<sup>c</sup>Department of Chemistry, Hacettepe University, 06800, Beytepe, Ankara, Turkey. E-mail: [bekir@hacettepe.edu.tr](mailto:bekir@hacettepe.edu.tr); Fax: +90 312 288 2163; Tel: +90 312 297 7975

<sup>d</sup>Department of Chemistry, Technical University of Istanbul, 34469 Maslak-Istanbul, Turkey. E-mail: [obek@itu.edu.tr](mailto:obek@itu.edu.tr); Fax: +90 216 3860824; Tel: +90 216 3479641

based circuits such as, displays, radio frequency identification tags, microelectronic logic, and some other small-scale integrated circuits.<sup>16</sup> Although the achieved performance of OFET thus far still cannot compete with the widely utilized inorganic analogues, *i.e.*, the amorphous hydrogenated silicon (a-Si:H) field effect transistors (FETs), significant progress has been made in the past decade toward understanding OFETs and realizing their industrial applications.<sup>17</sup> In order to further increase the number of modifiable physicochemical parameters of the subunit, we tried to obtain novel dimeric MPc, in which two Pc units are connected to each other with two  $-\text{CH}_2-$  bridges.

We now report the synthesis and characterization of new dimeric zinc(II) and cobalt(II) Pc complexes, and also their applications as electrocatalytic materials for dioxygen reduction and FET.

## 2. Results and discussion

### 2.1. Synthesis and characterization

The synthesis of **1** was performed beginning from 4-nitrophthalonitrile and 6,6'-methylenebis(2-(2-hydroxy-5-methylbenzyl)-4-methylphenol) in DMF at 50 °C by the catalysis of  $\text{K}_2\text{CO}_3$  under argon. The suitable dimeric MPcs **2** and **3** were prepared in dimethylaminoethanol with the appropriate metal salt. Both complexes are not soluble in any pure solvent. However, the addition of organic or mineral acid to the heterogeneous mixture of the MPc and solvent makes the compound soluble.

The formation of **1** was confirmed by the disappearance of the  $\text{NO}_2$  band of 4-nitrophthalonitrile at  $1350\text{ cm}^{-1}$  and the appearance of new intensive absorption band at  $1247\text{ cm}^{-1}$  belonging to Ar–O–Ar in the IR spectra. In the IR spectrum of **1**, the strong and characteristic  $\text{C}\equiv\text{N}$  band at  $2232\text{ cm}^{-1}$  disappeared after conversion to MPcs **2** and **3**. The intensive bands at  $1713$  and  $1715\text{ cm}^{-1}$  showed the  $\text{C}=\text{N}$  stretching vibrations for **2** and **3**, respectively. Furthermore, the peaks observed at  $1587$ – $1483\text{ cm}^{-1}$ ,  $1602$ – $1467\text{ cm}^{-1}$  and  $1604$ – $1403\text{ cm}^{-1}$  were attributed to unsaturated aromatic  $\text{C}=\text{C}$  double bond stretching frequencies for **1**, **2** and **3** respectively. Besides, the strongest peaks appearing at *ca.*  $1247$  for **1**,  $1219$  for **2** and  $1225\text{ cm}^{-1}$  for **3** in the spectra of the complexes were attributed to the aromatic ether bands ( $\text{C}-\text{O}-\text{C}$  intense stretching). The general shift trend of the complexes and metal sensitivity can also be found easily in this region. The peak at  $1086\text{ cm}^{-1}$  for **2** shifts to  $1103\text{ cm}^{-1}$  for **3** indicating that this vibration mode is metal sensitive.

Fig. 1 shows the UV-vis spectra of **2** and **3** in DMF and DMSO at varying concentrations within the range of  $1.73 \times 10^{-5}$ – $5.78 \times 10^{-7}\text{ mol dm}^{-3}$ . These spectra showed characteristic Q-band absorptions between 686 and 672 nm which were attributed to the  $\pi \rightarrow \pi^*$  transitions from the highest occupied molecular orbital (HOMO) to the lowest unoccupied molecular orbital (LUMO) of the Pc ring. The other bands (B) in the UV region within the range of 355–327 nm were observed due to the transitions from the deeper  $\pi$  levels to the LUMO. The spectrum of **3** in DMF or DMSO involved a broad Q band

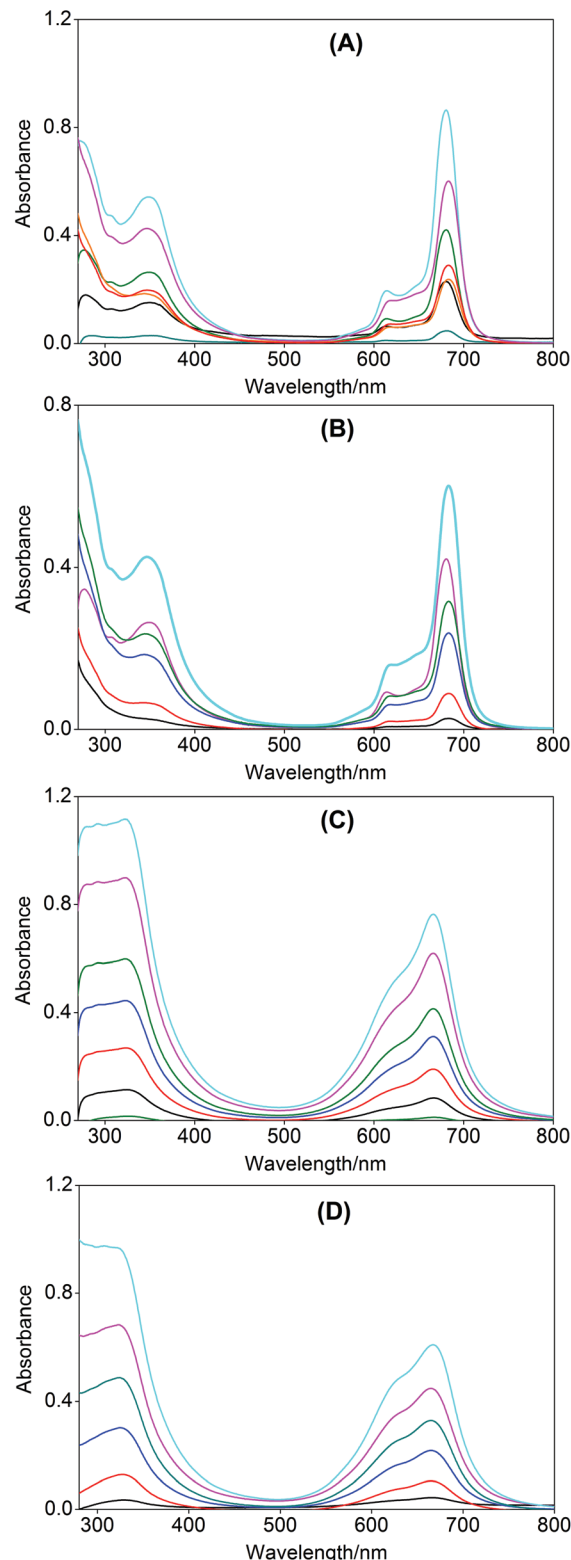


Fig. 1 UV-vis spectra of (A) **2** in DMF, (B) **2** in DMSO, (C) **3** in DMF and (D) **3** in DMSO within the range of  $1.73 \times 10^{-5}$ – $5.78 \times 10^{-7}\text{ mol dm}^{-3}$ .

absorption with a shoulder at the higher energy side, which is quite typical for intermolecularly interacting or aggregated metallo Pcs. The trend of Pcs to self-aggregate through

coplanar association of the Pc rings to form dimers and higher order aggregates is well known.<sup>18</sup> In general, Pc aggregation results in a decrease in intensity and broadening of the Q band, and increasing intensity of the Soret band corresponding to the monomeric species. However, As shown in Fig. 1C and 1D, while the solutions of **3** in DMF and DMSO were diluted from  $1.73 \times 10^{-5} \text{ mol dm}^{-3}$  to  $5.78 \times 10^{-7} \text{ mol dm}^{-3}$ , the absorption ratio of Q and satellite bands did not change as in the literature<sup>19</sup> and the broadness of the spectrum did not decrease. This observation strongly suggests that the broad Q band absorption in the spectrum of **3** is due to the intramolecular interactions between the two CoPc units in the ball-type dinuclear cobalt Pc,  $\text{Co}_2\text{Pc}_2$ . On the other hand, the electronic absorption spectra of **2** in DMF and DMSO displayed a sharp Q band absorption with its vibrational component at the higher energy side Fig. 1A and 1B which is characteristic not only for non-aggregated or intermolecularly interacting, but also for intramolecularly non-interacting MPCs.

MALDI-TOF mass spectra of **1** and **3** are given in Fig. 2 and 3, respectively. These spectra were recorded in dithranol with better intensity than the other conventional MALDI matrices. Although the high resolution spectra could be accumulated for **1**, it was not possible to obtain reasonable peak intensities for the cobalt complex **3** because of the short life times of the protonated molecular ion in reflectron mode mass spectrometer. For **1**, sodiated and potasiated ion signals were observed in the case of the protonated ion signal due to the low affinity of the ligand to the proton compared to the sodium and potassium. It was concluded that compound **1** was synthesized and purified perfectly. The MALDI-TOF mass spectra of **3** suggested that many fragmentation occurred and the fragment ions mainly followed each other with 224 Da masses representing side chain fragmentation and also high intense dimer and trimer of the complex (data not shown). The fragmentation may be attributed to dominant aggregation in the crystal form of the MALDI sample.

Fig. 4 shows MALDI-TOF mass spectra of **2** in 2,5-dihydroxybenzoic acid which had better intensity than those recorded with other conventional MALDI matrices. Beside the

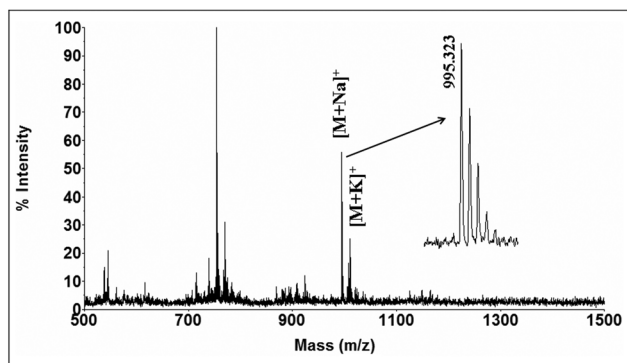


**Fig. 2** Positive ion and reflectron mode MALDI-TOF mass spectrum of  $\text{C}_{63}\text{H}_{40}\text{N}_8\text{O}_4$  **1** in dithranol MALDI matrix using nitrogen laser (at 337 nm wavelength) accumulating 100 laser shots. Inset spectrum shows expanded molecular mass region of the sodium adduct of the ligand.

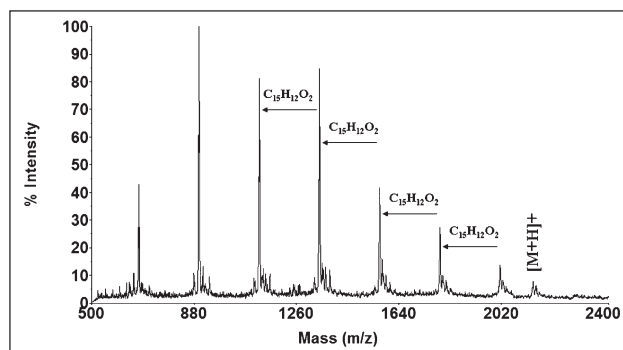


**Fig. 3** Positive ion and linear mode MALDI-TOF mass spectrum of **3** in dithranol MALDI matrix using nitrogen laser (at 337 nm wavelength) accumulating 100 laser shots.

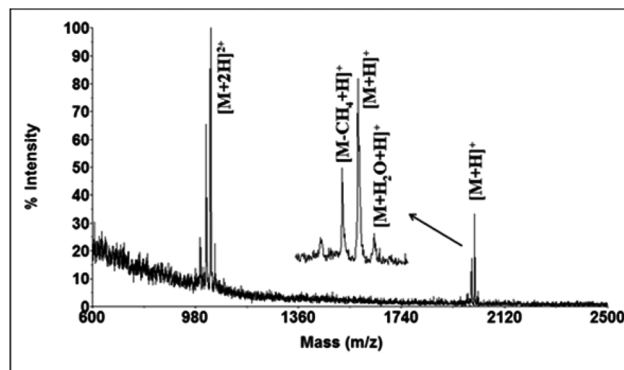


**Fig. 4** Positive ion and linear mode MALDI-TOF mass spectrum of  $\text{C}_{126}\text{H}_{80}\text{N}_{16}\text{O}_8\text{Zn}_2$  **2** in 2,5-dihydroxybenzoic acid MALDI matrix using nitrogen laser (at 337 nm wavelength) accumulating 100 laser shots.

protonated ion signal, water adduct signal also was observed at reasonably high intensity. However, methane loss from the protonated molecular ion signal was observed at high intensity because of the possibly available methane leaving group of the complex. On the other hand, the peaks for doubly charged ions of all water adducts, protonated molecular ion and major fragment ions after methane elimination were observed with really high intensity. Mass of the protonated ion signal confirmed that the complex was synthesized perfectly. It was also concluded from the clean MALDI-TOF mass spectrum that the complex was purified completely.

The  $^1\text{H}$  NMR spectrum of **1** displayed characteristic signals for  $-\text{CH}_3$  substituted to phenyl as two singlets at 2.11 and 2.19 ppm, and  $-\text{CH}_2-$  protons binding of two phenyls as singlet at 3.42 ppm. The peak at 6.70–8.27 ppm showed the presence of aromatic protons.

## 2.2. Electrochemistry

The voltammetric measurements were carried out on platinum in DMSO for **2** and **3**. The relevant data are given in Table 1. Typical cyclic and differential pulse voltammograms of **2** are shown in Fig. 5A. It displayed two reductions at  $E_{1/2} = -0.72 \text{ V}$  and  $E_{1/2} = -1.15 \text{ V}$  versus SCE, and an oxidation at  $E_{1/2} = 0.78 \text{ V}$

**Table 1** The electrochemical data for **2** and **3** in DMSO<sup>a</sup>

Complex	Redox processes	$E_{1/2}$ (V)	$\Delta E_p$ (V)	$\Delta E_{1/2}$ (V)	$\Delta E_s$ (V)
2	$[\text{Zn(II)Pc(-1)}]_2^{2+}/[\text{Zn(II)Pc(-2)}]_2$ (O1)	0.78	0.04	1.50	
	$[\text{Zn(II)Pc(-2)}]_2/[\text{Zn(II)Pc(-3)}]_2^{2-}$ (R1)	-0.72	0.03		
	$[\text{Zn(II)Pc(-3)}]_2^{2-}/[\text{Zn(II)Pc(-4)}]_2^{4-}$ (R2)	-1.15	0.20		
3	$[\text{Co(II)Pc(-2)-Co(II)Pc(-1)}]^+ / [\text{Co(II)Pc(-2)}]_2$ (O1)	0.52	—	0.80	0.34
	$[\text{Co(II)Pc(-2)}]_2 / [\text{Co(II)Pc(-2)-Co(I)Pc(-2)}]^-$ (R1)	-0.28	0.08		
	$[\text{Co(II)Pc(-2)-Co(I)Pc(-2)}]^- / [\text{Co(I)Pc(-2)}]_2^{2-}$ (R2)	-0.62	0.08		
	$[\text{Co(I)Pc(-2)}]_2^{2-} / [\text{Co(I)Pc(-2)-Co(I)Pc(-3)}]^{3-}$ (R3)	-1.07	0.10		
	$[\text{Co(I)Pc(-2)-Co(I)Pc(-3)}]^{3-} / [\text{Co(I)Pc(-3)}]_2^{4-}$ (R4)	-1.35	0.10		

<sup>a</sup> Potentials are reported with respect to the SCE.  $E_{1/2}$  values were measured by cyclic voltammetry [ $E_{1/2} = (E_{pa} + E_{pc})/2$ ] and/or differential pulse voltammetry. The peak separation values ( $\Delta E_p = E_{pa} - E_{pc}$ ) are reported at 0.100 V s<sup>-1</sup> except R2 at 0.500 V s<sup>-1</sup> for **2**.  $\Delta E_{1/2}$  is the potential difference between the first oxidation and first reduction potentials. It represents the HOMO-LUMO gap for **2**, but the charge transfer transition for **3** involving redox-active metal centers.  $\Delta E_s$  indicates mixed-valence splitting energy for the relevant split redox couple.

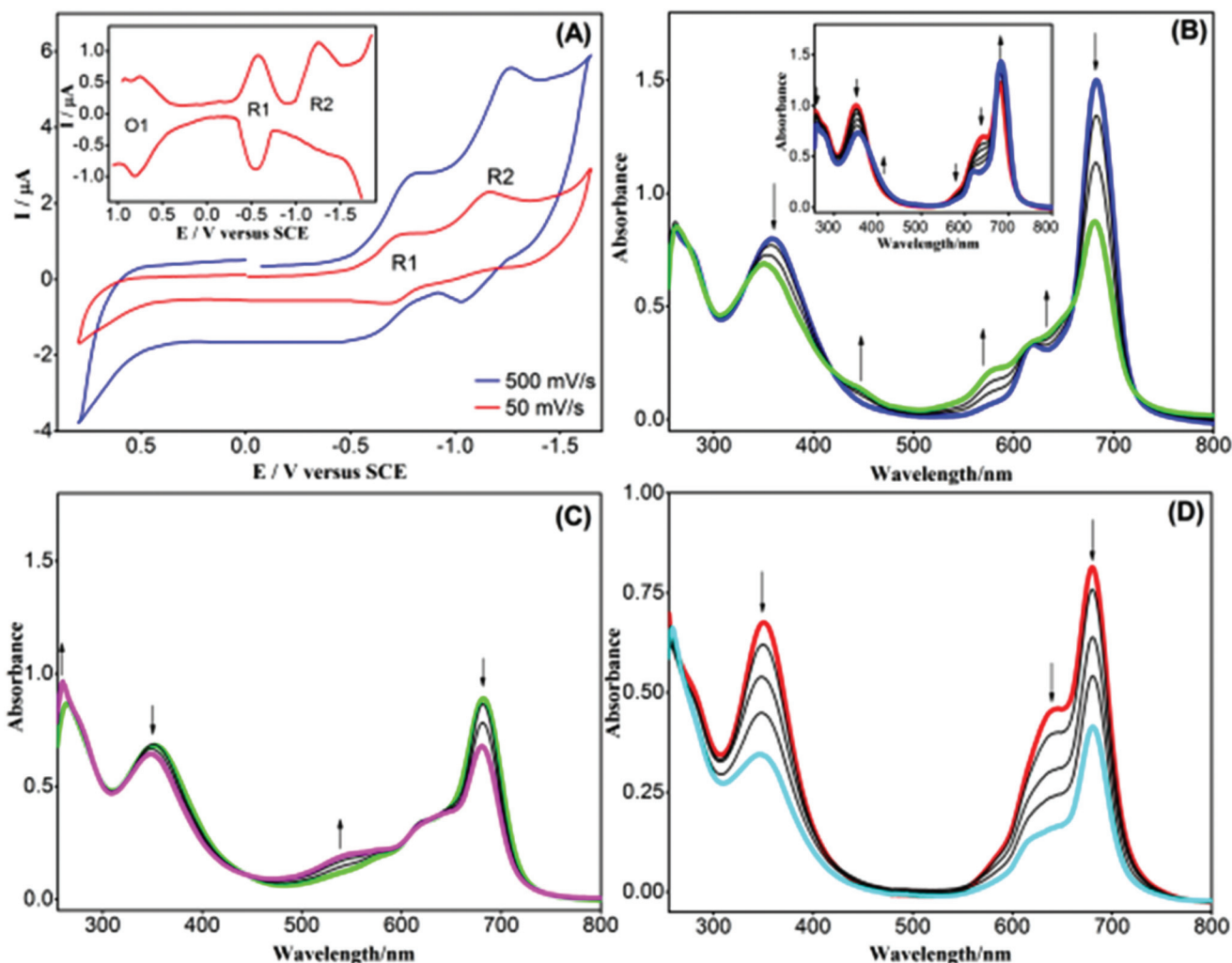


**Fig. 5** (A) Cyclic and differential pulse (inset) voltammograms of **2** on Pt and *in situ* UV-vis spectral changes during the controlled-potential electrolysis of the solution of **2** at (B) -0.85 V (two groups of spectral changes were observed; inset shows the first group) (C) -1.30 V and (D) 0.95 V *versus* SCE in DMSO/TBAP.

*versus* SCE which could be detected only by differential pulse voltammetry. The CPC studies showed that each reduction process of **2** involves the transfer of two electrons per the molecule. The comparison of the area under each peak in differential pulse voltammogram of **2** implies that the oxidation

process also involves the transfer of two electrons per the molecule. The transfer of two electrons for each redox process suggests that there is not considerable interaction between two Pc rings and/or two metal centers in this complex, and thus two MPc units electrochemically react at the same potentials.

The similarity of the redox behaviour of **2** to mononuclear Pcs supports this idea.<sup>20</sup> However, the peaks in the voltammograms are somewhat broad, which can be attributed to the presence of weak intramolecular interactions. The overall splitting of the molecular orbitals with a high degree on going from the monomeric to dimeric, trimeric or oligomeric Pcs depending on the intramolecular interactions between the two MPc units are expected to occur only in the case that these units are positioned in face to face orientation with a small distance between them. Thus, it may be concluded that two MPc units in **2** are approximately planar in nature or far to each other if they are cofacial. As shown in (Fig. 5A), the anodic component of the R2 couple is not observed at low scan rates suggesting that the electrochemically produced species during the second reduction process are not stable. *In situ* spectroelectrochemical measurements were also carried out during the electrolysis of the solution of **2** in DMSO/TBAP at suitable constant potentials corresponding to its redox processes. The spectrum monitored at the beginning of the electrolysis at  $-0.85$  V *versus* SCE corresponding to R1 involves a band at 640 nm at the blue side of the main Q band at 680 nm (the inset in Fig. 5B). In dimeric Pcs, intramolecular coupling between the rings causes a band at the red side of the characteristic Q band, at around 630 nm. Thus, the band at 640 nm can be attributed to the intramolecular interactions between the two MPc units in **2**. Upon the application the potential of

$-0.85$  V, two groups of spectral changes with different isosbestic points were recorded. During the first group of spectral changes, the absorptions of the bands at 640, 351 and 258 nm decrease while that of the main Q-band at 680 nm increases (the inset in Fig. 5B). These spectral changes are associated by the formation well-defined isosbestic points at 670, 534 and 384 nm. The disappearance of the band at 640 nm may be due to the decrease in the intramolecular interactions, probably as a result of the conformational changes in the molecule before the electron transfer process upon the applied electrical potential.

During the second group of spectral changes, the absorptions of the main Q-band around 680 nm and the B-band at 360 nm decrease whereas the absorption within the range of 418–660 nm increases and a new band at 576 nm forms (Fig. 5B). These spectral changes especially decrease in the Q-band without shift and the formation of a new band between 500 and 600 nm are characteristic for ligand-based electron transfer processes.<sup>21</sup> Similarly, the formation of a new band at 542 nm and decrease in the Q-band without shift during the second reduction R2 at  $-1.30$  V *versus* SCE corresponds to a ligand-based process (Fig. 5C). Although the first oxidation of **2** could be monitored by differential pulse voltammetry, the electrolysis at the constant potential of 0.95 V *versus* SCE led to its decomposition, evidenced by decrease in absorption of all bands (Fig. 5D).

The voltammetric behaviour of **3** was considerably different from that of **2**. This compound showed one-electron redox

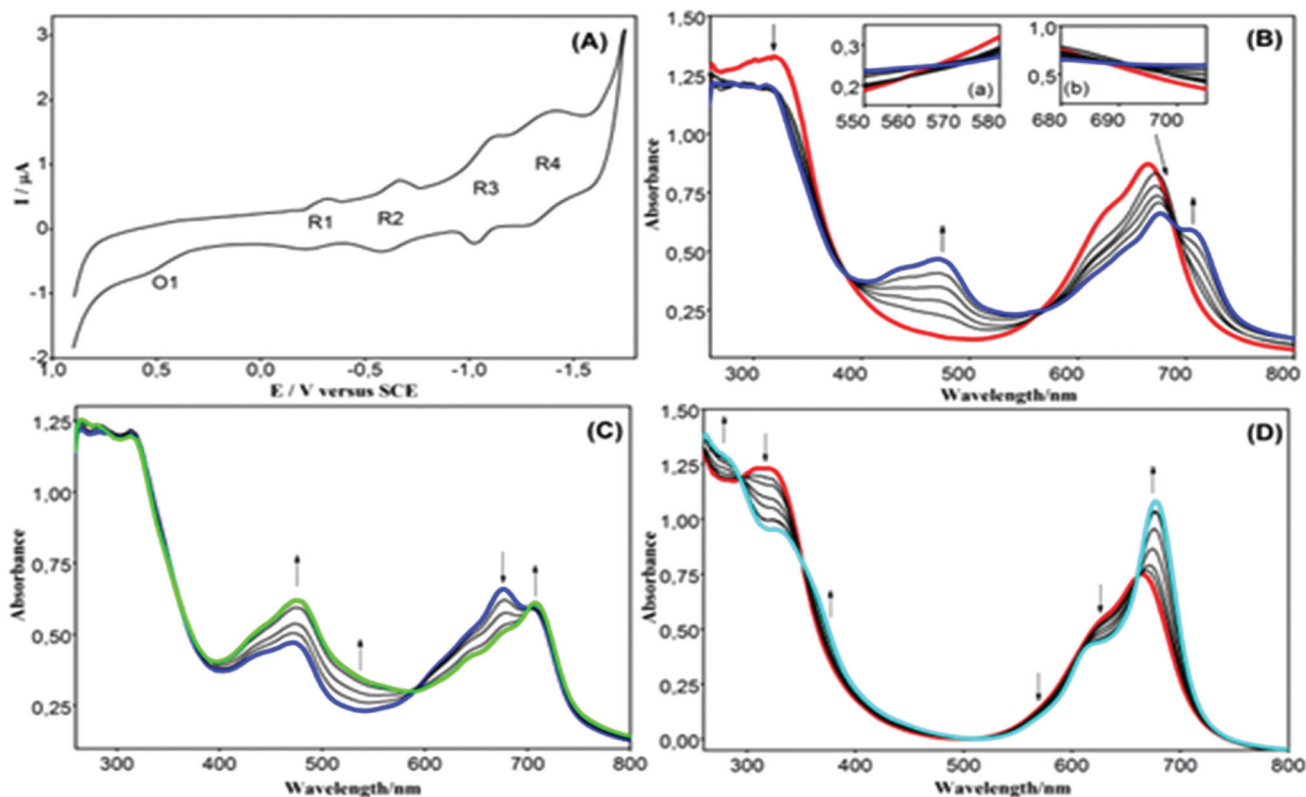


**Fig. 6** (A) Cyclic voltammogram of **3** at  $0.100$  V  $s^{-1}$  on Pt and *in situ* UV-vis spectral changes during the controlled-potential electrolysis of the solution of **3** at (B)  $-0.80$  V (insets a and b show the formation of various isosbestic points within the ranges of 560–580 nm and 680–710 nm, respectively, rather than a well-defined single isosbestic point (C)  $-1.50$  V and (D)  $0.65$  V *versus* SCE in DMSO/TBAP.

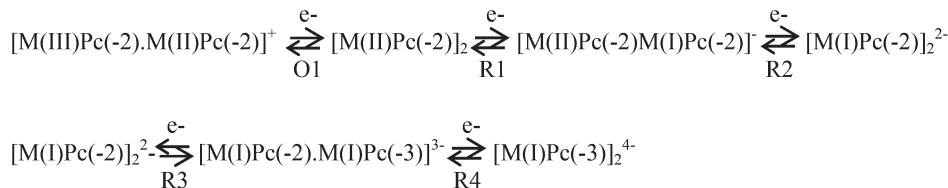


Chart 1 Electrode reactions for **3**. M: Co.

processes. A typical cyclic voltammogram for this compound is shown in Fig. 6A.

The transfer of one electron in each step indicates that the splitting of the molecular orbitals occurs as a result of the remarkable interaction between the two Pc rings and/or two metal centers in **3**, and thus the redox processes of each Pc ring and/or metal center in this complex occur at different potentials. This behaviour implies that two MPc units in **3** are planar, at least partially, rather than being planar since the remarkable interaction between the molecular orbitals of two Pcs and/or two metal centers, in a dimer cause considerable changes in redox potentials, compared with corresponding mono Pcs and non-interacting planar dimers. The electrode reactions and the mixed-valence species formed by these reactions are schematically illustrated in (Chart 1) for **3**. The mixed-valence splitting,  $\Delta E_s$ , values in V for the redox processes of **3** are presented in (Table 1). These values give evidence of the delocalization of charge among the two Pc rings and/or two metal centers in **3**, and thus the formation of electrochemically stable oxidized and reduced mixed-valence species. Although the splitting of the Co(II)/Co(I) redox couple into two waves as  $[\text{Co}(\text{II})\text{Pc}(-2)]_2/[\text{Co}(\text{II})\text{Pc}(-2)\text{Co}(\text{I})\text{Pc}(-2)]^-$  and  $[\text{Co}(\text{II})\text{Pc}(-2)\text{Co}(\text{I})\text{Pc}(-2)]^-/[\text{Co}(\text{I})\text{Pc}(-2)]_2^{2-}$ , and the Pc(-2)/Pc(-3) couple as  $[\text{Co}(\text{I})\text{Pc}(-2)]_2^{2-}/[\text{Co}(\text{I})\text{Pc}(-2)\cdot\text{Co}(\text{I})\text{Pc}(-3)]^{3-}$  and  $[\text{Co}(\text{I})\text{Pc}(-2)\cdot\text{Co}(\text{I})\text{Pc}(-3)]^{3-}$  in **3** was detected clearly by cyclic voltammetry measurements, it was not possible to monitor the spectra of the mixed-valence reduced species the during spectroelectrochemical measurements under the conditions of constant-potential electrolysis. However, upon reduction at  $-0.80$  V *versus* SCE, the formation of various isosbestic points within the ranges of 560–580 nm and 680–710 nm rather than a well-defined single isosbestic point imply the formation of short-lived mixed-valence species of  $[\text{Co}(\text{II})\text{Pc}(-2)\text{Co}(\text{I})\text{Pc}(-2)]^-$  (the insets in Fig. 6B). The remarkably broad band and especially the shoulder at its blue side in the first spectrum in (Fig. 6B), monitored at the beginning of the electrolysis of the solution of **3** in DMSO/TBAP, are probably due to the intramolecular interactions between the two MPc units. The decrease in the absorptions of the main Q-band at 665 nm with the red-shift to 677 nm and in its shoulder around 625 nm is accompanied by the formation of the new bands at 473 and 706 nm. These spectral changes are characteristic for Co(II)/Co(I) reduction.<sup>21a-c,22</sup> Upon reduction at  $-1.50$  V *versus* SCE, the main Q-band nearly disappears and the intensity of the new band at 473 nm increases (Fig. 6C). These spectral changes are accompanied by considerable increase in absorption within the range of 400–500 nm which is typical for Pc ring-

reduction.<sup>22</sup> The formation of various isosbestic points within the ranges of 580–590 nm rather than a single one should also be due to the formation of short-lived mixed-valence species of  $[\text{Co}(\text{I})\text{Pc}(-2)\cdot\text{Co}(\text{I})\text{Pc}(-3)]^{3-}$  (the inset in (Fig. 6C). Fig. 6D shows the spectral changes recorded during the electrolysis at 0.65 V *versus* SCE. The red-shifting of the main Q-band at 665 nm to 677 nm with the increase the absorption is characteristic for metal-based Co(II)/Co(III) oxidation<sup>22,23</sup> and can be attributed to  $[\text{Co}(\text{II})\text{Pc}(-2)]_2/[\text{Co}(\text{III})\text{Pc}(-2)\cdot\text{Co}(\text{II})\text{Pc}(-2)]^+$  process since O1 involves the transfer of one electron per the molecule. The formation of well-defined isosbestic points at 294, 350 and 660 nm supports the oxidation of  $[\text{Co}(\text{II})\text{Pc}(-2)]_2$  species to only  $[\text{Co}(\text{III})\text{Pc}(-2)\cdot\text{Co}(\text{II})\text{Pc}(-2)]^+$  ones. Some studies in the literature showed that while some binuclear and tetranuclear Pcs formed metal-centered type or ring-centered type mixed-valence species, some of them did not.<sup>14b,5-7,9,15,23</sup> The difference was attributed mainly to the presence or absence of axial ligands, respectively inhibiting or facilitating the close approach of the rings, and to the other steric factors. The least strongly coupled systems included some zinc complexes of binuclear Pcs. Thus, weak intramolecular interactions observed for **2** in this study are consistent with the literature.<sup>14b,23</sup> Mixed-valence ring reduction, Pc(-2)·Pc(-3), was observed previously only in strongly coupled silicon species,<sup>23c</sup> but was not unequivocally observed with the other bridged binuclear species. The presence of an extra  $\pi$ -electron usually repels the  $\pi$ -electron density in the other ring and therefore inhibits formation of these species unless they are constrained to lie close together. The large splitting values for the silicon species was attributed to the shorter Pc...Pc contacts than in the bridged systems. The splitting of the redox processes of the Pc ring and metal center for **3** in this study may be attributed to the deviation from planarity due to flexible  $-\text{CH}_2-$  group in the bridging units.

The electrocatalytic activities of the ball-type Pc complexes **2** and **3** towards oxygen reduction reaction (ORR) was also tested since some articles reported by our group showed that electrocatalytic activities of ball-type dinuclearmetallopCs for ORR are encouraging in general for applicability in fuel cells.<sup>8b,c,12,13,23</sup> The ring and disk polarization curves of a rotating ring disk electrode (RRDE), disk of which was modified by a mixture of the relevant Pc complex with Vulcan XC-72 (VC) and Nafion (Nf), in O<sub>2</sub>-saturated 0.5 M H<sub>2</sub>SO<sub>4</sub> aqueous electrolyte solution (Fig. 7), have been monitored and then the catalytic performance has been characterized the by the onset potential ( $E_o$ ) where the oxygen reduction current begins to increase, the limiting diffusion disk current density ( $J_L$ ) and

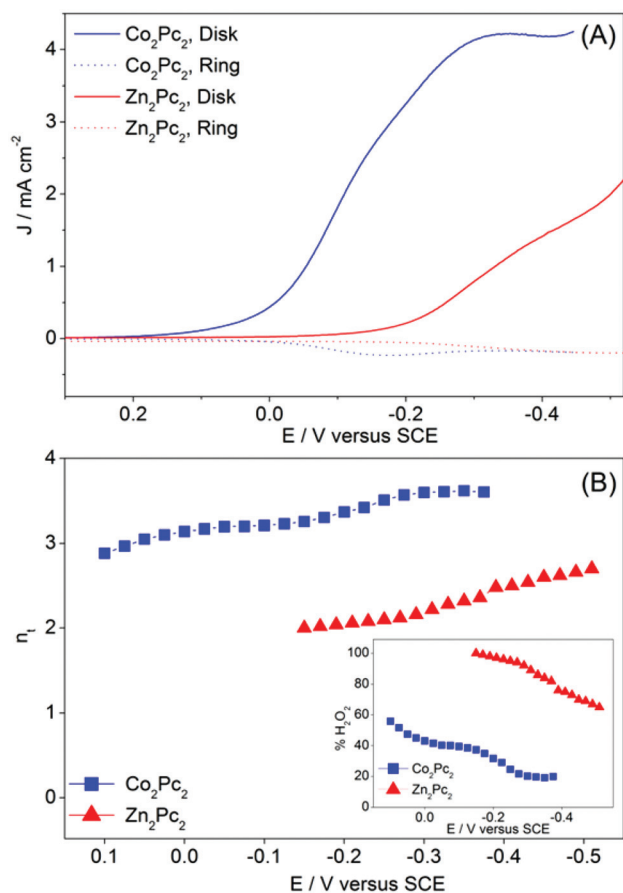


**Fig. 7** (A) RRDE polarization curves for the electrocatalytic ORR at  $0.005 \text{ V s}^{-1}$  on VC/Nf/ $M_2\text{Pc}_2$  modified rotating (2500 rpm) glassy carbon disk electrode and platinum ring electrode in  $\text{O}_2$ -saturated  $0.5 \text{ M H}_2\text{SO}_4$ . (B) Number of total electrons exchanged for VC/Nf/ $M_2\text{Pc}_2$  modified electrodes (inset shows  $\% \text{H}_2\text{O}_2$  produced in ORR as a function of disk potential ( $E_{\text{ring}} = 0.95 \text{ V vs. SCE}$ )).

the half-wave potential ( $E_{1/2}$ ). The disk potential at which the current density reaches to  $0.100 \text{ mA cm}^{-2}$  was taken as  $E_0$ . Table 2 lists the electrocatalytic performances of 2 and 3. It also includes the catalytic activities of some previously reported ball-type dinuclear cobalt Pcs with dicumarol,<sup>13</sup> 4,4'-(octahydro-4,7-methano-5H-inden-5-ylidene)bisphenol,<sup>12</sup> dithioerythritol,<sup>23a</sup> cyclopentylsilanoxy-polyhedral oligomeric silsesquioxanes,<sup>23b</sup> and pentaerythritol,<sup>8b,c</sup> bridging units for comparison. The ORR catalyzed by 3 displays two reduction waves (Fig. 7A). The limit current densities for 3 is much higher than that of 2. In addition,  $E_0$  value for 3 is much more positive than that of 2. Therefore, the catalytic performance of ball-type dinuclear cobalt  $\text{Pc}_2$  towards ORR is much better than that of ball-type dinuclear zinc  $\text{Pc}_2$ . ORR in acidic medium can be either a four-electron process to form water or a two-electron reduction to form hydrogen peroxide. The ring currents in RRDE voltammetry measurements, carried out with a VC/Nf/ $M_2\text{Pc}_2$  modified glassy carbon disk electrode and a platinum ring electrode polarized at  $0.95 \text{ V versus SCE}$  were used to determine the number of electrons peroxide and thus water selectivity. The  $n_t$  and the percentage of hydrogen

**Table 2** Electrocatalytic properties of 2 and 3, and the comparison with previously reported<sup>8b,c,12,13,23a,b</sup> dinuclear ball-type cobalt phthalocyanines

Complex	$E_0$ for ORR <sup>a</sup> /V	$J_L$ for ORR <sup>b</sup> /mA cm <sup>-2</sup>	$E_{1/2}$ for ORR/V	Ref.
Zn <sub>2</sub> Pc <sub>2</sub> 2	-0.15	1.06	-0.30	tw <sup>c</sup>
Co <sub>2</sub> Pc <sub>2</sub> 3	0.06	2.54	-0.07	tw <sup>c</sup>
Co <sub>2</sub> Pc <sub>2</sub> <sup>d</sup>	0.45	1.66	-0.21	13
		0.92	0.35	
Co <sub>2</sub> Pc <sub>2</sub> <sup>e</sup>	0.11	4.66	-0.15	12
Co <sub>2</sub> Pc <sub>2</sub> <sup>f</sup>	0.10	3.30	-0.14	23a
Co <sub>2</sub> Pc <sub>2</sub> <sup>g</sup>	0.68	4.27	0.41	23b
		2.17	-0.19	
Co <sub>2</sub> Pc <sub>2</sub> <sup>h</sup>	0.25	4.50	-0.09	8c
Co <sub>2</sub> Pc <sub>2</sub> <sup>i</sup>	0.51	4.84	0.05	8c

<sup>a</sup> The potential at which the current density reaches to  $0.100 \text{ mA cm}^{-2}$  was taken as the onset potential. <sup>b</sup> The limiting diffusion current density at 2500 rpm. <sup>c</sup> This work. <sup>d</sup> Dicumarol bridged. <sup>e</sup> 4,4'-(Octahydro-4,7-methano-5H-inden-5-ylidene)bisphenylbridged. <sup>f</sup> Dithioerythritol-bridged. <sup>g</sup> Cyclopentylsilanoxy-polyhedral oligomeric silsesquioxanes bridged. <sup>h</sup> Pentaerythritol-bridged. <sup>i</sup> Pentaerythritol-bridged with hepta-decafluorodecyl substituents.

peroxide produced at a given potential was determined by the following equations:<sup>24</sup>

$$n_t = 4I_D[I_D + (I_R/N)] \quad (1)$$

$$\% \text{H}_2\text{O}_2 = 100(4 - n_t)/2 \quad (2)$$

where  $N$ ,  $I_D$ , and  $I_R$  are the collection efficiency, disk current and ring current, respectively. Fig. 7B shows the  $n_t$  and percentage of hydrogen peroxide and water generated at different potentials. The occurrence of two waves during ORR in (Fig. 7A) and the  $n_t$  values higher than 3 for the first wave in (Fig. 7B) for 2-catalyzed ORR implies that it probably occurs *via* peroxo species, producing water as the main product and some hydrogen peroxide as the side product. The second wave, appearing at considerably negative potentials probably corresponds to the reduction of hydrogen peroxide to water. The absolute ring current decreases simultaneously while the disk current increases during the appearance of the second wave (Fig. 7A), which confirms that hydrogen peroxide produced at the first step as the side product is further reduced to water during the second wave.

According to some authors, electrocatalytic reduction of oxygen on MPcs takes place through a redox-catalysis type of process where oxygen binding ability and the redox potential of the central metal ions play a critical role.<sup>25</sup> The metal ion in the center of Pc ring is oxidized by oxygen molecule during its adsorption and thus reduces it. The metal centers in 3 are redox-active while those in 2 are redox-inactive, and thus neither oxidized nor reduced under the conditions of electrocatalytic measurement, as judged from their *in situ* spectroelectrochemical measurements and well-known electrochemical behaviour.<sup>20</sup> So, the higher catalytic activity of 3 as compared to 2 can be attributed to its redox-active metal centers and their ability to bind dioxygen molecule due to distinctive coordinating properties. This type of improved catalytic activity towards ORR was also suggested for various

covalently linked porphyrine dimers in the literature.<sup>26</sup> However, it should be noted that the catalytic performance of previously reported ball-type cobalt Pcs with dicumarol,<sup>13</sup> 4,4'-(octahydro-4,7-methano-5*H*-inden-5-ylidene)bisphenol,<sup>12</sup> dithioerythritol,<sup>23a</sup> cyclopentyl disilanoxy-polyhedral, oligomeric silsesquioxanes,<sup>23a</sup> and pentaerythritol,<sup>8b,c</sup> bridging units for ORR was higher than that of **3**. This can be attributed to the difference in the distance between the two CoPc units and the flexibility of the molecules.

### 2.3. Characteristics of OFETs

In Fig. 8, the drain–source current  $I_{DS}$  is plotted as a function of the drain–source voltage  $V_{DS}$  for different gate–source voltages  $V_{GS}$  applied to ITO electrode, which acted as a gate. From the plots, the linear and saturation regions can be seen clearly with the increase of drain–source voltage. At low drain–source voltages, the drain–source current follows Ohm's law, and is proportional to drain–source voltage. As the drain–source voltage increased, the voltage, measured relative to the source, along the channel increases from the 0 to  $V_{DS}$ . Thus the voltage between the gate and points along the channel

decreases from  $V_{GS}$  at the source end to  $V_{GS}-V_{DS}$  at the drain end. Since the channel is no longer of uniform depth; rather, the channel take the tapered form being deepest at the source end and shallowest at the drain end. As  $V_{DS}$  is increased more, the channel becomes more tapered and its resistance increases correspondingly. Thus, the output characteristic ( $I_{DS}-V_{DS}$  plot) does not continue as a straight line. This situation is known as pinch-off of the conductive channel of the transistor. Therefore it can be said that the observed saturation in  $I_{DS}$  is due to pinch-off of the channel. Fig. 8 also shows that the drain–source current is effectively modulated by gate voltage, the drain current of both the 2-based OFET and 3-based OFET increases with negative gate voltages. These data show that the devices exhibit a field effect with operation in a p-type accumulation mode.

The relation between the  $I_{DS}$  and the  $V_{DS}$  and  $V_{GS}$  in the linear and saturation regions is given by eqn (3) and (4), respectively.<sup>27</sup>

$$I_{DS} = \frac{W}{L} C_i \mu_F (V_{GS} - V_t) V_{DS} - \frac{1}{2} V_{DS}^2 \quad (3)$$

$$I_{DS} = \frac{W}{2L} C_i \mu_F (V_{GS} - V_t)^2 \quad (4)$$

where  $\mu_F$  is the field-effect mobility,  $W$  and  $L$  are the channel width and length, respectively,  $C_i$  is the capacitance of the dielectric layer, and  $V_t$  is the threshold voltage.

The most important parameter describing the performance of an OFET is the field-effect mobility that indicates how easy the charge carriers can drift under the influence of electric field, and most efforts to date have been devoted to its enhancement. The mobility of the transistors can be obtained in different ways. In this work, the values of the mobility for both transistors were extracted from the saturation region operation of the devices. For this purpose, the  $I_{DS}$  currents at constant  $V_{DS} = -55$  V were obtained from the response curves (Fig. 8). The square roots of these currents were then plotted as function of the gate voltage. Fig. 9 shows this plot for 2/PVA OFET. With the aid of eqn (2), from the slope of the linear portion of Fig. 9 the  $\mu_F$  values were found as  $2.8 \times 10^{-3} \text{ cm}^2 \text{ V}^{-1} \text{ s}^{-1}$  and  $7.3 \times 10^{-3} \text{ cm}^2 \text{ V}^{-1} \text{ s}^{-1}$  for **2** and **3**, respectively.

It was observed that the obtained mobility values of the studied Pc-based OFETs are higher than the mobilities of CuPc-based FET using PVA as gate insulator<sup>28</sup> with the value of  $2.2 \times 10^{-4} \text{ cm}^2 \text{ V}^{-1} \text{ s}^{-1}$  and CuPc-OFET using polymethyl methacrylate (PMMA) dielectric layer with the mobility of  $0.2 \times 10^{-4} \text{ cm}^2 \text{ V}^{-1} \text{ s}^{-1}$ .<sup>29</sup>

## 3. Experimental

### 3.1. Materials

All chemicals used were of reagent grade quality. 4-Nitrophthalonitrile and 6,6'-methylenebis(2-(2-hydroxy-5-methylbenzyl)-4-methylphenol) were purchased from TCI and used as received. All reactions were carried out under a dry argon atmosphere unless otherwise noted. The target compound **1** was

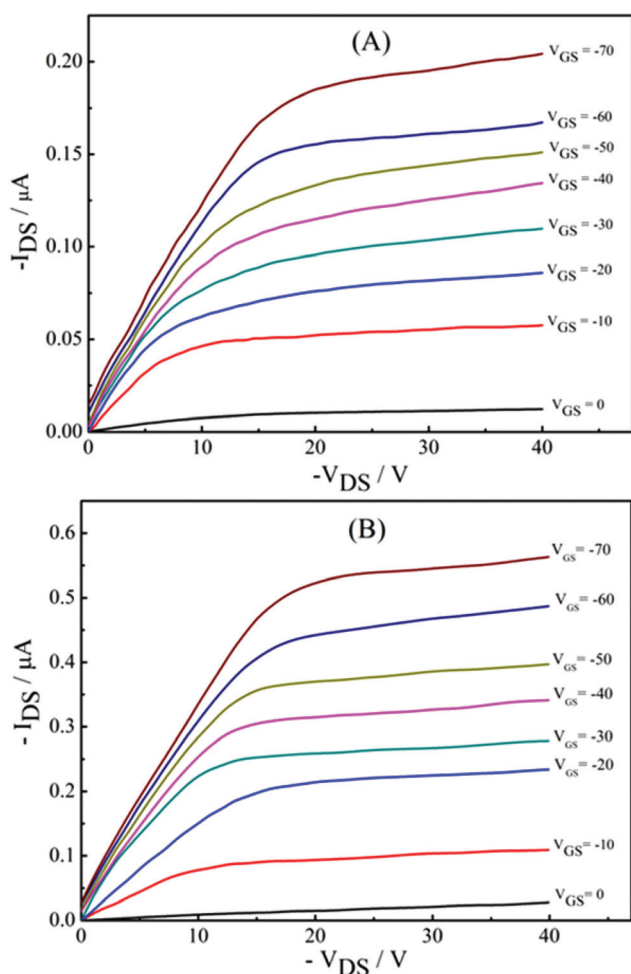


Fig. 8 The output characteristics ( $I_{DS}-V_{DS}$ ) of (A) **2** (80 nm)/PVA (300 nm) OFET and (B) **3** (80 nm)/PVA (300 nm) OFET at different  $V_{GS}$  from 0 V to  $-70$  V.

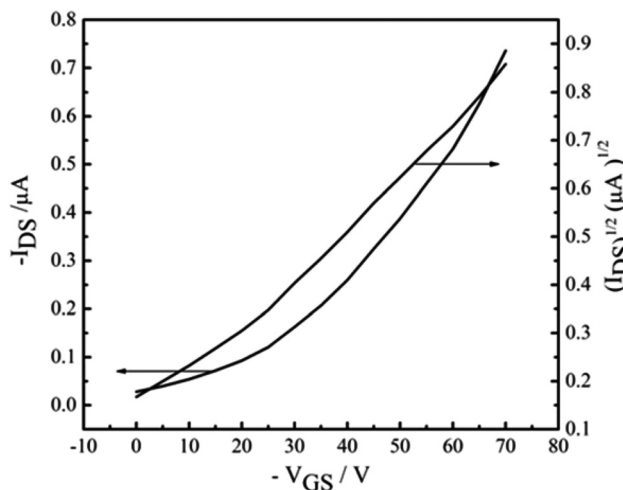


Fig. 9 Dependence of  $I_{DS}$  current and its square root on the  $V_{GS}$  voltage of the 3-based device.

synthesized and purified according to the methods described previously in literature,<sup>30</sup> and was isolated by column chromatography on silica gel 60. The Pc compounds were purified successively by washing with hot acetic acid, water and methanol, respectively, and extracted in the Soxhlet with acetone. The melting points of the Pc compounds were found to be higher than 300 °C.

### 3.2. Equipment

IR spectra were recorded on a Perkin Elmer Spectrum One FTIR (ATR sampling accessory) spectrophotometer. UV-vis spectra were recorded on a Shimadzu UV-1601 UV-vis spectrometer. <sup>1</sup>H-NMR spectra were recorded on a Varian UNITY INOVA 500 MHz spectrometer. Elemental analyses were performed by the Instrumental Analysis Laboratory of the TUBITAK, Marmara Research Centre. Mass spectra were acquired on a Voyager-DE™ PRO MALDI-TOF mass spectrometer (Applied Biosystems, USA) equipped with a nitrogen UV-Laser operating at 337 nm. Spectra were recorded in reflection mode for 1 and linear mode for 2 and 3 with average of 100 shots.

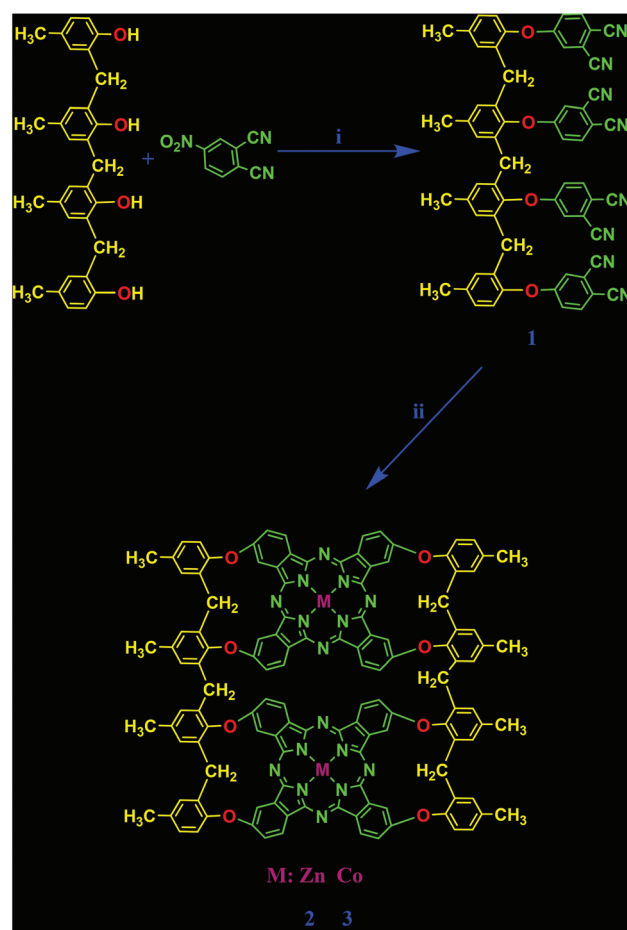
### 3.3. Synthesis

**3.3.1. 4,4'-(6,6'-Methylenebis(2-(2-(3,4-dicyanophenoxy)-5-methylbenzyl)-4-methylphenylene)]bis(oxy)diphthalonitrile 1.** A mixture of 6,6'-methylenebis(2-(2-hydroxy-5-methylbenzyl)-4-methylphenol) (0.93 g, 2 mmol), 4-nitrophthalonitrile (1.37 g, 8 mmol) and anhydrous  $K_2CO_3$  (1.65 g, 12 mmol) in 40 mL of anhydrous dimethylformamide (DMF) in a flask was sealed after removal of  $O_2$ . After the reaction mixture was stirred at 50 °C for 72 h, the mixture was poured into icy water and the formed precipitate was filtered off, washed by using water and dried under the vacuum at 50 °C for 48 h. The crude product was purified by column chromatography with silica gel eluting with  $CH_2Cl_2$ . Compound 1 is soluble in  $CH_2Cl_2$ ,

$CHCl_3$ , THF, DMF and DMSO. Mp: 253 °C. Yield: 1.94 g (79.34%).

Anal. calculated for  $C_{63}H_{40}N_8O_4$  C, 77.76; H, 4.14; N, 11.52%; found C, 77.34; H, 4.16; N, 11.67%. IR (ATR),  $\nu_{max}(cm^{-1})$ : 3104, 3075, 3040, 2924, 2854, 2232, 1587, 1568, 1483, 1247. <sup>1</sup>H NMR (400 MHz, DMSO- $d_6$ )  $\delta$  ppm; 2.11(s, 6H), 2.19(s, 6H), 3.42(s, 6H), 6.70, 6.78, 6.81, 6.83, 6.908(s, 8H), 7.02(m, 6H), 7.33(d,  $J = 2.46$  Hz, 2H), 7.82(m, 2H), 7.90(d,  $J = 8.77$ , 2H), 8.27(s, 2H). MALDI-TOF-MS:  $m/z$  995.32 ( $M + Na$ )<sup>+</sup> (Scheme 1).

**3.3.2. 2',10',16',24'-[6,6'-Methylenebis[2(2-hydroxy)-5-methylbenzyl]-4-methyl]-bis(oxydiphthalocyaninato-dizinc(II)) 2.** A mixture of 1 (0.48 g, 0.50 mmol) and  $Zn(OAc)_2 \cdot 2H_2O$  (0.11 g, 0.50 mmol) was heated with 2 mL of dry DMA in a sealed tube. The mixture was kept at 180 °C for 3 h under oxygen free atmosphere. After cooling to room temperature, the reaction mixture was treated with methanol and filtered. The raw green product was washed by several solvents to purify and extracted in Soxhlet with acetone for 12 h. The crude product was purified by column chromatography on silica gel eluting with THF and AcOH of 5% in DMF. The complex 2 is not soluble in any common solvent. However, it is soluble in DMF or DMSO after



Scheme 1 (i)  $K_2CO_3$ , DMF, 50 °C, 72 h; (ii) (a)  $Co(OAc)_2 \cdot 4H_2O$ , DMA, 180 °C, 20 min, (b)  $Zn(OAc)_2 \cdot 2H_2O$ , DMA, 180 °C, 20 min.

dropping acetic acid (about 1%) to the solvent. Mp > 300 °C. Yield: 214.08 mg (41.30%).

Anal. calculated for  $C_{126}H_{80}N_{16}O_8Zn_2$ : C, 73.32; H, 3.91; N, 10.83%; found C, 73.56; H, 3.96; N, 10.78%. IR (ATR),  $\nu_{\max}(\text{cm}^{-1})$ : 2919, 1713, 1602, 1467, 1220, 1086, 1039, 746, 438. MALDI-TOF-MS:  $m/z$  ( $M - \text{CH}_4 + \text{H}$ )<sup>+</sup>, 2073.49 ( $M + \text{H}$ )<sup>+</sup>, ( $M + \text{H}_2\text{O} + \text{H}$ )<sup>+</sup>. UV-vis(DMF):  $\lambda_{\max}$  (nm), ( $\log \epsilon$ ): 355 (5.10), 623 (4.76), 680 (5.33) (Scheme 1).

**3.3.3. 2',10',16',24'-{6,6'-Methylenebis[2(2-hydroxy)-5-methylbenzyl]-4-methyl-bis(oxydiphthalocyaninato-dicobalt(II))** **3**. The synthesis and the purification of **3** was achieved by the same route used for **2**. A mixture of **1** (0.48 g, 0.50 mmol) and  $\text{Co}(\text{OAc})_2 \cdot 4\text{H}_2\text{O}$  (0.088 g, 0.50 mmol) was heated with 2 mL of dry DMA in a sealed tube. The solubility of blue complex **3** is the same of **2**. Mp > 300 °C. Yield: 240.14 mg (46.55%).

Anal. calculated for  $C_{126}H_{80}Co_2N_{16}O_8$ : C, 72.87; H, 3.88; N, 10.79%; found C, 72.59; H, 3.91; N, 10.64%. IR (ATR),  $\nu_{\max}(\text{cm}^{-1})$ : 2921, 1715, 1604, 1554, 1470, 1403, 1225, 1103, 1056, 752, 443. MALDI-TOF-MS:  $m/z$  2063.50 ( $M + \text{H}$ )<sup>+</sup>, UV-vis (DMF):  $\lambda_{\max}$  (nm), ( $\log \epsilon$ ): 320 (4.32), 612 (3.89), 668 (4.26) (Scheme 1).

### 3.3.4. MALDI sample preparation

MALDI matrix, dithranol was prepared in ACN:H<sub>2</sub>O:DMSO mixture in 1 : 1 : 1 v/v/v ratio at a concentration of 10 mg mL<sup>-1</sup>. MALDI samples for **1** and **3** were prepared by mixing sample solutions (2 mg mL<sup>-1</sup> in ACN:H<sub>2</sub>O:DMSO mixture in 1 : 1 : 1, v/v/v ratio) with the matrix solution (1:10 v/v) in a 0.5 mL Eppendorf® micro tube. Finally 0.5 µL of this mixture was deposited on the sample plate, dried at room temperature and then analyzed. On the other hand MALDI matrix, 2,5-dihydroxybenzoic acid was prepared in ACN:H<sub>2</sub>O mixture in 1 : 1 v/v ratio at a concentration of 10 mg mL<sup>-1</sup> and acidified with trifluoroacetic acid (0.1%). MALDI samples for **2** were prepared by mixing sample solutions (2 mg mL<sup>-1</sup> in water:DMSO in 1 : 1 ratio by v/v containing 0.1% trifluoroacetic acid) with the matrix solution (1 : 10 v/v) in a 0.5 mL Eppendorf® micro tube. Finally 0.5 µL of this mixture was deposited on the sample plate, dried at room temperature and then analyzed.

### 3.3.5. Electrochemistry

Cyclic voltammetry and differential pulse voltammetry measurements were carried out with a PAR Model VersoStat II Potentiostat/Galvanostat controlled by an external PC, and utilizing a three electrode configuration at 25 °C. Tetrabutylammonium perchlorate (TBAP) (Electrochemical grade, Fluka Chemical Co.) was used as the supporting electrolyte in extra pure DMSO. A saturated calomel electrode (SCE) was employed as the reference electrode and separated from the bulk of the solution by a fritted glass bridge filled with the solvent-supporting electrolyte mixture. The ferrocene/ferrocenium couple ( $\text{Fc}/\text{Fc}^+$ ) was used as an internal standard, but potentials were reported with respect to SCE. The working electrode was platinum in the measurements. A platinum spiral wire was used as the auxiliary electrode. Solutions containing the complexes were deoxygenated by a stream of high-purity nitrogen for at

least 20 min prior to running the experiment, and the solution was protected from air by a blanket of nitrogen during the experiment. For the controlled-potential coulometry (CPC) studies, a platinum gauze working electrode, a platinum wire counter electrode separated with a bridge, a SCE as reference electrode, and a model 377/12 synchronous stirrer were used.

The spectroelectrochemical measurements were carried out by an Agilent Model 8453 diode array spectrophotometer equipped with the potentiostat/galvanostat and utilizing a three-electrode configuration of thin layer quartz spectroelectrochemical cell at 25 °C. The working electrode was transparent Pt gauze. Pt wire counter electrode separated by a glass bridge and a SCE reference electrode separated from the bulk of the solution by a double bridge were used.

Ultra pure water and extra pure sulphuric acid (Merck) were used to prepare the electrolyte solution in electrocatalytic measurements. VC (Cabot Co.), 5% Nf solution (Aldrich), extra pure ethyl alcohol (Merck), VC supported platinum particles (ElectroChem, Inc.) and the Pc compounds were used in catalyst preparation. Glassy carbon disk electrode, glassy carbon disk-platinum ring electrode and a polishing kid for these electrodes were purchased from Pine Instruments. Two Gamry Reference 600 potentiostats, controlled by an external PC and utilizing a four electrode configuration at 25 °C, were connected as a bipotentiostat to control the ring and disk potentials and to collect the respective currents during RRDE experiments. A Pine Instrument Company AFMSRCE modulator speed rotator was employed in the experiments. The working electrode was a glassy carbon disc (5.61 mm dia) and a platinum ring leading to a collection efficiency,  $N = 37\%$ . The disk potential was swept at 0.005 V s<sup>-1</sup>, the ring potential was held at 0.95 V *versus* SCE and the rotation rate of the electrode was 2500 rpm. These experiments were carried out in 0.5 M H<sub>2</sub>SO<sub>4</sub> oxygen saturated electrolyte at 25 °C. In order to disperse the catalysts on a carbon support, a mixture of the Pc compound, VC and 5 wt% Nf solution in absolute ethanol was prepared and ultrasonically homogenized for half an hour. A given volume of this ink was deposited using a micropipette onto a freshly polished glassy carbon electrode leading to a catalyst loading of 106 µg cm<sup>-2</sup>. In order to obtain a total coverage of the glassy carbon surface, the deposited drop of ink was dried with pulsed air at ambient temperature to evaporate the solvent quickly. Each voltammogram was recorded with a freshly prepared electrode due to the possible catalyst degradation in acid medium.

### 3.3.6. OFET fabrication

We fabricated OFETs having a bottom-gate and top source-drain contact geometry. To fabricate the OFETs used in this work, an indium tin oxide (ITO)-coated glass substrate was used as gate electrode. Before using, the ITO coated substrates were cleaned by ultrasonic treatment in acetone, isopropyl alcohol, and deionized water. After being dried by Ar gas, ITO surfaces were treated by UV-ozone for 20 min. Then, on the top of ITO surface, polyvinyl alcohol (PVA) was dissolved in distilled water, with thicknesses of 300 nm was spin coated at

1500 rpm. After drying the PVA film at 115 °C for 1 h in a vacuum oven, a solution of Pcs in DMF, with a concentration of  $3 \times 10^{-3}$  M, was spun on top of PVA film rotating at 2500 rpm. Ellipsometric technique was used to measure the thickness of the dielectric layer and the Pc films. Subsequently, the deposited films (80 nm) were thermally annealed at 140 °C for 30 min to evaporate the solvent. Finally, on the top of Pc layer, gold source and drain contacts with thickness of 110 nm was evaporated by thermal evaporation at the pressure below  $10^{-5}$  mbar. The source and drain electrodes were formed through the shadow mask. The electrical characteristics of these devices were measured in air. For electrical measurements a Keithley 617 programmable electrometer and a Keithley 2400 sourcemeter were used.

## Conclusions

In this work, the novel dimeric MPcs, **2** and **3** have been obtained from tetrakis-phthalonitrile in dimethylaminoethanol with the proper metal salts. Electrochemical and *in situ* spectroelectrochemical measurements suggested that while complex **2** displays only Pc-based two-electron redox processes, compound **3** shows both metal-based and Pc-based one-electron processes. It was concluded from the electrocatalytic measurements suggested that the catalytic performance of  $\text{Co}_2\text{Pc}_2$  **3** towards ORR is much higher than that of  $\text{Zn}_2\text{Pc}_2$  **2**. The catalytic measurements displayed that the nature of the central metals in a dinuclear ball-type Pc complex has a remarkable influence on its catalytic activity towards ORR.

Compounds **2** and **3** have been applied as semiconducting layer in OFETs. The results proved that spin coated films of these compounds can be used as the semiconducting layers of OFETs functioned as p-channel accumulation devices. From the analysis of the electrical characteristics of the OFETs, it was observed that the 2-based and 3-based OFETs with polymeric gate insulator presented satisfactory p-type electrical characteristics with high mobilities. Such high performance OFETs are a great impetus for realizing large-area, low-cost and flexible displays.

## Acknowledgements

We thank the Turkish Academy of Sciences (TUBA) and Marmara University, Scientific Research Commission (Project No: FEN-A-130612-0220) for their support.

## Notes and references

- Phthalocyanines, Properties and Applications*, ed. C. C. Leznoff and A. B. P. Lever, VCH Publications, New York, 1989, 1993, 1993, 1996, vol. I, II, III, and IV; *Phthalocyanine. Chemistry and Functions*, ed. H. Shirai and N. Kobayashi, IPC, Tokyo, 1997.
- C. C. Leznoff, H. Lam, S. M. Marcuccio, W. A. Nevin, P. Janda, N. Kobayashi and A. B. P. Lever, *J. Chem. Soc., Chem. Commun.*, 1987, 699.
- J. Jiang, K. Kasuga and D. P. Arnold, in *Supramolecular Photosensitive and Electroactive Materials*, ed. H. S. Nalwa, Academic Press, New York, 2001, ch. 2, p. 113.
- (a) N. Kobayashi, M. Numao, R. Kondo, S. Nakajima and T. Osa, *Inorg. Chem.*, 1991, **30**, 2241; (b) N. Kobayashi, *J. Chem. Soc., Chem. Commun.*, 1991, 1203; (c) D. Lelievre, L. Bosio, J. Simon, J. J. Andre and F. Bensebaa, *J. Am. Chem. Soc.*, 1992, **114**, 4475.
- T. Ceyhan, A. Altındal, A. R. Özkaya, M. K. Erbil, B. Salih and Ö. Bekaroğlu, *Chem. Commun.*, 2006, 320.
- Z. Odabaş, A. Altındal, A. R. Özkaya, M. Bulut, B. Salih and Ö. Bekaroğlu, *Polyhedron*, 2007, **26**, 695.
- M. Özer, A. Altındal, A. R. Özkaya, B. Salih, M. Bulut and Ö. Bekaroğlu, *Eur. J. Inorg. Chem.*, 2007, 3519.
- (a) M. Özer, A. Altındal, B. Salih, M. Bulut and Ö. Bekaroğlu, *Tetrahedron Lett.*, 2008, **49**, 896; (b) M. Özer, A. Altındal, A. R. Özkaya and Ö. Bekaroğlu, *Dalton Trans.*, 2009, 3175; (c) İ. Koç, M. Özer, A. R. Özkaya and Ö. Bekaroğlu, *Dalton Trans.*, 2009, 6368.
- Z. Odabas, A. Altındal, A. R. Özkaya, M. Bulut, B. Salih and Ö. Bekaroğlu, *Polyhedron*, 2007, **26**, 3505.
- S. Altun, A. Altındal, A. R. Özkaya, M. Bulut and Ö. Bekaroğlu, *Tetrahedron Lett.*, 2008, **49**, 4483.
- M. S. Ağırtaş, A. Altındal, B. Salih, S. Saydam and Ö. Bekaroğlu, *Dalton Trans.*, 2011, **40**, 3315.
- A. Sengül, H. Z. Doğan, A. Altındal, A. R. Özkaya, B. Salih and Ö. Bekaroğlu, *Dalton Trans.*, 2012, **41**, 7559.
- Ü. Salan, A. Altındal, A. R. Özkaya, B. Salih and Ö. Bekaroğlu, *Dalton Trans.*, 2012, **41**, 5177.
- (a) N. Kobayashi, Y. Yanagisawa, T. Osa, H. Lam and C. C. Leznoff, *Anal. Chem.*, 1990, **6**, 813; (b) N. Kobayashi, H. Lam, W. A. Nevin, P. Janda, C. C. Leznoff and A. B. P. Lever, *Inorg. Chem.*, 1990, **29**, 3415; (c) N. Kobayashi, H. Lam, W. A. Nevin, P. Janda, C. C. Leznoff, T. Koyama, A. Monden and H. Shirai, *J. Am. Chem. Soc.*, 1994, **116**, 879.
- T. Ceyhan, A. Altındal, A. R. Özkaya, Ö. Çelikbıçak, B. Salih, M. K. Erbiland and Ö. Bekaroğlu, *Polyhedron*, 2007, **26**, 4239.
- S. R. Forrest, *Nature*, 2004, **428**(6986), 911.
- Y. Gao, P. Ma, Y. Chen, Y. Zhang, Y. Bian, X. Li, J. Jiang and C. Ma, *Inorg. Chem.*, 2009, **48**, 45.
- A. W. Snow, in *The Porphyrin Handbook*, ed. K. M. Kadish, K. M. Smith and R. Guillard, Academic, San Diego, 2003, vol. 17, p. 129.
- X. Huang, F. Zhao, Z. Li, Y. Tang, F. Zhang and C. H. Tung, *Langmuir*, 2007, **23**, 5167.
- A. B. P. Lever, E. R. Milaeva and G. Speier, in *Phthalocyanines, Properties and Applications*, ed. C. C. Leznoff and A. B. P. Lever, VCH, Weinheim, 1993, vol. 3, pp. 1–69.
- (a) A. Koca, A. R. Özkaya, Y. Arslanoğlu and E. Hamuryudan, *Electrochim. Acta*, 2007, **52**(9), 3216; (b) A. Koca, A. R. Özkaya, M. Selçukoğlu and E. Hamuryudan,

- Electrochim. Acta*, 2007, **52**(7), 2683; (c) M. Özer, A. Altındal, A. R. Özkaya, M. Bulut and Ö. Bekaroğlu, *Polyhedron*, 2006, **25**(18), 3593; (d) R. D. George, A. W. Snow, J. S. Shirk and W. R. Barger, *J. Porphyrins Phthalocyanines*, 1998, **2**, 1; (e) P. C. Martin, M. Gouterman, B. V. Pepich, G. E. Renzoni and D. C. Schindele, *Inorg. Chem.*, 1991, **30**(17), 3305.
- 22 (a) C. C. Leznoff, H. Lam, W. A. Nevin, N. Kobayashi, P. Janda and A. B. P. Lever, *Angew. Chem., Int. Ed. Engl.*, 1987, **26**, 1021; (b) V. Manivannan, W. A. Nevin, C. C. Leznoff and A. B. P. Lever, *J. Coord. Chem.*, 1988, **19**, 139; (c) W. A. Nevin, W. Liu, S. Greenberg, M. R. Hempstead, S. M. Marcuccio, M. Melnik, C. C. Leznoff and A. B. P. Lever, *Inorg. Chem.*, 1987, **26**, 891; (d) D. W. DeWulf, J. K. Lelend, B. L. Wheeler, A. J. Bard, D. A. Batzel, D. R. Dininny and M. E. Kenney, *Inorg. Chem.*, 1987, **26**, 266.
- 23 (a) T. Ceyhan, A. Altındal, A. R. Özkaya, B. Salih and Ö. Bekaroğlu, *Dalton Trans.*, 2010, **39**, 9801; (b) T. Ceyhan, A. Altındal, A. R. Özkaya, B. Salih and Ö. Bekaroğlu, *Dalton Trans.*, 2009, 10318; (c) D. W. DeWulf, J. K. Lelend, B. L. Wheeler, A. J. Bard, D. A. Batzel, D. R. Dininny and M. E. Kenney, *Inorg. Chem.*, 1987, **26**, 266.
- 24 (a) K. H. Schweikart and M. Hanack, *Eur. J. Org. Chem.*, 2000, 2551; (b) E. M. Maya, P. Vazquez, T. Torres, L. Gobbi, F. Diedrich, S. Pyoand and L. Echegoyen, *J. Org. Chem.*, 2000, **65**, 823; (c) N. Kobayashi, *Coord. Chem. Rev.*, 2002, **227**, 129.
- 25 J. P. Randin, *Electrochim. Acta*, 1974, **19**, 83.
- 26 (a) J. P. Collman, M. Marrocco, P. Denisevich, C. Koval and F. C. Anson, *J. Electroanal. Chem.*, 1979, **101**, 117; (b) J. P. Collman, N. H. Hendricks, C. R. Leidner, E. Ngameni and M. L'Her, *Inorg. Chem.*, 1988, **27**, 387; (c) R. R. Durand, C. S. Bencosme, J. P. Collman and F. C. Anson, *J. Am. Chem. Soc.*, 1983, **105**, 2710; (d) H. Y. Liu, I. Abdalmuhdi, C. K. Chang and F. C. Anson, *J. Phys. Chem.*, 1985, **89**, 665; (e) H. Y. Liu, M. J. Weaver, C. B. Wang and C. K. Chang, *J. Electroanal. Chem.*, 1983, **145**, 439; (f) C. K. Chang, H. Y. Liu and I. Abdalmuhdi, *J. Am. Chem. Soc.*, 1984, **106**, 2725; (g) J. P. Collman, F. C. Anson, S. Bencosme, A. Chong, T. Collins, P. Denisevich, E. Evitt, T. Geiger, J. A. Ibers, G. Lameson, Y. Konai, C. Koval, K. Meier, P. Okaley, R. Pettman, E. Schmittou and J. Sessler, in *Organic Synthesis Today and Tomorrow*, ed. B. M. Trost and C. R. Hutchinson, Pergamon Press, Oxford, 1981, pp. 29–45.
- 27 S. M. Sze, *Physics of Semiconductor Devices*, Wiley, New York, 1981.
- 28 H. Kawaguchi, M. Taniguchi and T. Kawai, *Synth. Met.*, 2008, **158**, 355.
- 29 J. Puigdollers, C. Voz, M. Fonrodona, S. Cheylan, M. Stella, J. Andreu, M. Vetter and R. Alcubilla, *J. Non-Cryst. Solids*, 2006, **352**, 1778.
- 30 J. G. Young and W. Onyebuago, *J. Org. Chem.*, 1990, **55**, 2155.